Energy Storage and Conversion 2025, 3(3), 3366.
doi: https://doi.org/10.59400/esc3366

Article

Thermodynamic modeling of the Power-to-Gas technology with methane and hydrogen as a chemical storage

Peter Ivanov *, **Andrey Zhuk**

Joint Institute for High Temperatures, Russian Academy of Sciences, 125412 Moscow, Russia

*** Corresponding author:** Peter Ivanov, peterivanov1248@gmail.com

CITATION

Ivanov P, Zhuk A. Thermodynamic modeling of the Power-to-Gas technology with methane and hydrogen as a chemical storage. Energy Storage and Conversion. 2025; 3(3): 3366. https://doi.org/10.59400/esc3366

ARTICLE INFO

Received: 1 May 2025
Revised: 10 June 2025
Accepted: 16 June 2025
Available online: 10 July 2025

Abstract: A novel toolset is developed for the thermodynamic modeling of the direct and reverse energy conversion processes in the scope of Power-to-Gas technology, which means the use of gases as chemical storage of electricity. The direct process is well commercialized, electrolysis of water, or of vapor in the high temperature version. The reverse process, up to recently, has been considered unreasonable due to the high demand for electrolysis hydrogen for other processes. An appearance of highly efficient convertors of chemical energy of gases into electricity, like solid oxide fuel cells (SOFC), claims to reconsider the Power-to-Gas technology as a whole, firstly from a thermodynamic point of view. It is done in this paper using a one-way conversion approach in terms of thermodynamic cycle and thermodynamic potentials. To deal with the heat flow through the energy conversion plants, the pinch analysis was used by means of composed TQ-diagrams for heat sources and heat sinks. The toolset was tested on two options of the technology with methane and hydrogen as chemical storage. Methane option, compared with hydrogen, seems to be thermodynamically more efficient, because there are two cases of thermally integrating the exothermal and endothermal processes: high temperature electrolysis (SOEC technology) with methanation, and the internal reforming of methane in SOFC.

Keywords: thermodynamic modeling; TQ-diagrams; Power-to-Gas; solid oxide fuel cells; internal conversion of methane

1. Introduction

Disbalance of energy demand and supply leads to the appearance of peak power plants, having lower cost and lower thermodynamic efficiency. But the large-scale deployment of intermittent renewable energy sources, like wind and solar, poses a growing challenge in terms of balancing energy demand and supply in real time, and the problem of temporary storage of electricity becomes a burning issue.

Early versions of energy storage are pumped hydro and compressed air energy storage (CAES) [1–4]. Recent developments are aimed at chemical storage. In the study of Buttler and Spliethoff [5], two technologies are discussed: PtG (Power-to-Gas) and PtL (Power-to-Liquids). As an example of PtL technology in Ghorbani et al.'s study [6, 7], an integrated structure is developed, separating CO_2 from the output smoke of a power plant using a chemical absorption unit via the post-combustion and liquefying CO_2 during off-peak hours, consuming power from the system. The low-temperature organic Rankine cycle and the gas turbine power production unit are used to produce power during peak hours. Storage of the electrolysis hydrogen in the liquefied form is considered in the study of Taghavi et al. [8,9].

The conception of PtG [10, 11] is closest to the natural status quo, considering that we produce energy mostly by means of burning a fuel—gas or oil. So, producing hydrogen by means of electricity, we are closing the reciprocal cycle of gas-energy conversion. This cycle consists of quite well-developed technologies [12]. The PtG technology deals with the electricity storage by means of the production of gases with high heating value—hydrogen and methane—during times of ample power supply, and the production of electricity to shave the peaks of system load using the stored gas. The feasibility of this reciprocal cycle is provided by the development of SOFC with high efficiency. The simplest set of processes in this cycle is: electrolysis to get hydrogen, storing the hydrogen, and producing electricity in SOFC.

Methane has some advantages to be a storage gas: it is a conventional fuel for power plants, goes through existing tubes of distribution and storage systems, less dangerous compared with hydrogen. Methane is produced from carbon dioxide using the Sabatier reaction [13–16]. Recently, this reaction has been under thorough investigation as a method of carbon dioxide utilization in order to stabilize the Earth's ecology. It is interesting for specialists in energy conversion too. There are a number of publications concerning the HELMETH project [17–20], based on the methanation of CO and CO_2, using electrolysis hydrogen. In NASA Sabatier reaction is considered to produce water and further oxygen from the expired air for the life sustenance of the orbital station [21].

In the current work, 4 processes from the PtG technology with storage gases, hydrogen and methane are considered:

- energy to methane: production of hydrogen by means of a solid oxide electrolyzer and its methanation using stored carbon dioxide;
- energy to hydrogen: production of hydrogen by means of a solid oxide electrolyzer;
- backup conversion from methane: electricity generation in the SOFC with internal conversion of methane using the stored methane;
- backup conversion from hydrogen: electricity generation in the SOFC using hydrogen and oxygen from corresponding storage vessels.

Electrochemical processes in the isobaric-isothermal environment are calculated using the one-way conversion approach in terms of thermodynamic cycles and processes and flow rates of mass (kg/s), of Gibbs energy, and enthalpy (kW). In more detail, this toolset is presented in our previous work [22]. Elements of this toolset are listed below.

1. Organization of the computational lay-out of the assembly with numbered working media.
2. Calculation of parameters of working media, based on mass and energy conservation and one-way conversions.
3. Calculation of TQ-diagrams of heat sources and heat sinks.
4. Organization of the composed TQ-diagrams for heat sources and heat sinks, and determination of the pitch-point temperature difference (allowed minimum is 35 K). The use of composed diagrams instead of individual ones overestimates a bit

the pitch-point temperature difference, but it is a usual practice in pilot modeling.

5. Identification of the points of thermodynamic cycle and of thermodynamic processes between them, as well as of the composing working media.
6. Calculation of composed thermodynamic potentials of the cycle points. Considering that here the main energy conversion processes are electrochemical reactions, it is necessary to track two potentials—Gibbs energy and enthalpy (the calculation of Brighton and Rankin cycles needs only one potential—enthalpy).
7. Determination of powers of cycle processes, including the useful power and the thermodynamic efficiency. Thermodynamic cycles determine the enthalpy effect of the electrochemical reaction ΔH and ΔG, the thermodynamic limit of the electric power (in kW). The real electric power of SOFC is determined using the load factor k ($N_{EL} = k\Delta G$). Here in calculations the value k = 0.85 was used. It was found to be justified in our previous work [23]. The process of electrolysis k is greater than unity. For the sake of simplicity, we used here the value $k = \Delta H/\Delta G$, which is based on the more advanced modeling.

In the first 4 sections of the current work, the developed toolset is used to model 4 schemes appearing in the Power-to-Gas technology with methane and hydrogen as storage gases.

Later, the resulting information is used for the estimation of the efficiency of the energy storage depending on the storage gas.

2. Energy storage gas—Methane

2.1. Computational lay-out (methane)

Figure 1 presents the computational lay-out of the installation used for energy storage into methane.

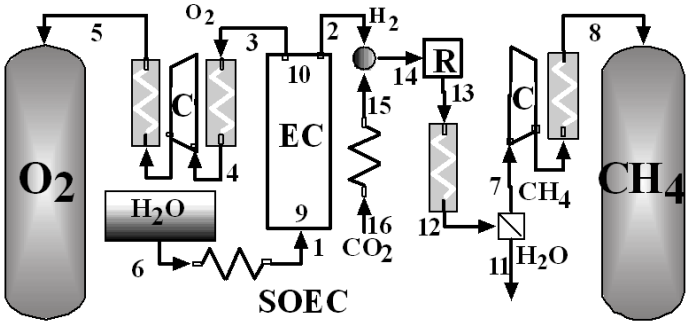

Figure 1. Computational lay-out of the installation for the energy storage into methane.

2.2. Parameters of working media (methane)

Table A1 of **Appendix A** specifies the Parameters of working media. Computations are performed using the individual matter properties from the database IVTANTHERMO [24].

2.3. Parameters of TQ-diagrams of heat sources and heat sinks (methane)

Table 1 lists the parameters associated with the TQ diagrams of both heat sources and heat sinks.

Table 1. Characteristics of heat sources and sinks of heat on **Figure 1**.

N	Working media	*m*, kg/s	*T1*, K	*T2*, K	*Q*, kW
Heat sinks:					
1	6–1	0.07206	288.0	1038	289.7
2	16–15	0.04401	323.0	1038	34.54
3		1.0	1038	1038	189.3
Heat sources:					
1	3–4	0.064	323.0	1073	49.06
2	4–5	0.064	323.0	672.8	21.75
3	4–5	0.064	323.0	672.8	21.75
4	13–12	0.05207	323.0	1073	99.87
5	7–8	0.01604	323.0	556.1	10.04
6	7–8	0.01604	323.0	556.0	10.04
7		1.0	1073	1073	189.3
8		1.0	429.8	430.0	121.8

Note:
Sinks 1 and 2 are the heating of water (steam) and CO_2 at the indicated places of lay-out. Sources 1 and 4 correspond to the cooling of oxygen and of the mixture of CH_4 with steam at the indicated places of lay-out.
Sources 2, 3, 5, 6 appear due to the cooling after steps of compression steps. Source 7 is the heat generated in the electrolyzer and transferred into the Stirling cycle for utilization as the sink 3. Heat discharge from the Stirling cycle becomes source 8.

2.4. Composed TQ-diagrams for heat sources and heat sinks (methane)

These diagrams are displayed at **Figure A1** in **Appendix A**.

2.5. Identification of the points of thermodynamic cycle (methane)

Table 2 identifies the points of thermodynamic cycle (column PTC) and of the involved working media (column WM).

Table 2. Thermodynamic cycle of conversion energy-methane.

PTC	WM	*m*, kg/s	*G*, kW	*H*, kW	Δ*G*, kW	Δ*H*, kW
A	16 + 6	0.1161	−1576	−1478		
B	16 + 1	0.1161	−2219	−1188	−642.6	289.7
C	15 + 1	0.1161	−2417	−1152	−198.9	36.47
D	15 + 9	0.1161	−2450	−1146	−32.89	5.912
E	15 + 10	0.1161	−1730	−153.0	720.3	992.9
F	15 + 2 + 3	0.1161	−1696	−153.0	34.07	0
G	14 + 3	0.1161	−1718	−153.0	−22.32	0
H	13 + 3	0.1161	−1667	−344.3	51.36	−191.2
I	12 + 3	0.1161	−1162	−444.1	505.1	−99.87
J	11 + 7 + 3	0.1161	−1157	−444.1	5.128	0
K	11 + 8 + 3	0.1161	−1144	−444.1	12.33	0
L	11 + 8 + 4	0.1161	−799.7	−493.2	344.8	−49.06
M	11 + 8 + 5	0.1161	−775.0	−493.2	24.67	0

Note: columns: PTC—points of thermodynamic cycle, WM—working media.

2.6. Parameters of the points of thermodynamic cycle (methane)

Flow rates and composed thermodynamic potentials of the cycle points are shown in columns m, G and H of **Table 2**. Their pointwise increments are in columns ΔG and ΔH.

2.7. Characteristics of thermodynamic cycle (methane)

Table 2 shows that between points A and D the heating of the system goes on. The transfer to point E is proper electrolysis—an electrochemical process, which requires electric power $d_G = \Delta G_E$ and the addition of heat up to $d_H = \Delta H_E$. Additional heat comes due to the imperfection of the process of electrolysis. The power of the electrolyzer is determined by the formula

$$N_{el} = kd_G \tag{1}$$

Where $d_G = \Delta G_E$ is ΔG from the row E of **Table 2**, is greater than 1 due to polarization overpotentials.

For the sake of simplicity, let us assume that the value of k makes N_{el} to be in accordance with the formula

$$N_{el} = \Delta H_E + Q_{H_2O} \tag{2}$$

where Q_{H_2O}—power to heat the steam from 1038 up to 1073 K, ΔH_E is ΔH from row *E* of **Table 2**.

Methanization goes on between points G and H, delivering the heat power 191.2 kW. Some part of this power is used to heat CO_2 before the reactor, and the remaining heat goes to the cycle of Stirling for the utilization.

The temperature of the heater of the Stirling cycle is assumed to be 35 K less than the operational temperature of the electrolyzer and reactor (1038 K). The temperature of the cooler (430 K) is selected to make the pitch-point temperature difference between the composed TQ-diagrams of heat sources and heat sinks equal to 35 K. Stirling cycle efficiency is calculated using the Shambadal-Novikov formula [25]:

$$\eta = 1 - \sqrt{T_0/T_1} \tag{3}$$

where T_0—temperature of cooler, T_1—temperature of heater.

So, the total power of installation is composed of the following items (in kW):

- electrolyzer 998.8
- oxygen compressor 43.5
- methane compressor 20.08
- heat utilization −67.46

  Total 994.9

3. Energy storage gas—Hydrogen

3.1. Computational lay-out (hydrogen option)

Figure 2 depicts the computational lay-out of the installation employed for energy storage into hydrogen.

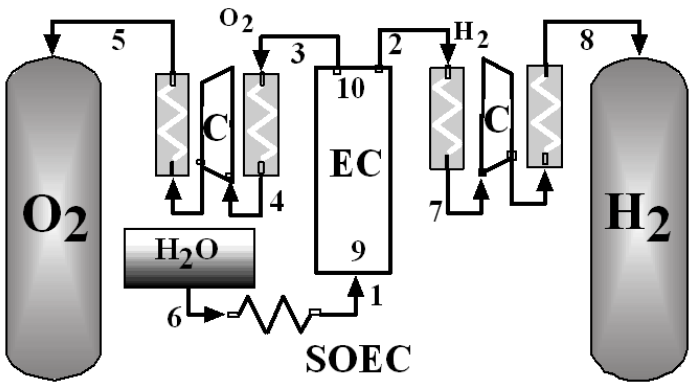

Figure 2. Computational lay-out of the installation for the energy storage into hydrogen.

3.2. Parameters of working media (hydrogen option)

Table A2 of **Appendix A** specifies the parameters of working media.

3.3. Parameters of TQ-diagrams of heat sources and heat sinks (hydrogen option)

The heat sources and heat sinks involved in the **Figure 2** configuration are defined by their TQ-diagram parameters and characteristics, as listed in **Table 3.**

Table 3. Characteristics of sources and sinks of heat on **Figure 2**.

N	Working media	*m*, kg/s	*T1*, K	*T2*, K	*Q*, kW
Heat sinks:					
1	6–1	0.05477	288.0	374.0	143.9
2	6–1	0.07206	374.0	1038	100.3
Heat sources:					
1	3–4	0.064	323.0	1073	49.06
2	4–5	0.064	323.0	672.8	21.75
3	4–5	0.064	323.0	672.8	21.75
4	2–7	0.008063	323.0	1073	88.7
5	7–8	0.008063	323.0	696.9	43.76
6	7–8	0.008063	323.0	696.9	43.76

Note:
Sink 1—water evaporation, 2–heating of the steam up to 1038K.
Sources 1 and 4 correspond to the cooling of oxygen and hydrogen at the indicated places of lay-out. Sources 2, 3, 5, 6 appear due to the cooling after steps of compression.

3.4. Composed TQ-diagrams for heat sources and heat sinks (hydrogen option)

Composed TQ-diagrams for heat sources and heat sinks are displayed in **Figure A2** in the **Appendix A**. Heat, provided by the cooling of electrolysis products, is not enough to boil the water; therefore, in order to keep the pitch-point temperature difference between composed TQ-diagrams for heat sources and heat sinks greater than or equal to 35 K, it is necessary to boil 24% of water, spending electric power.

3.5. Thermodynamic cycle of energy storage into hydrogen (hydrogen option)

Identification of the points of thermodynamic cycle and of the involved working media is done in columns PTC and WM of **Table 4**.

Table 4. Thermodynamic cycle of conversion energy-hydrogen.

PTC	WM	*m*, kg/s	*G*, kW	*H*, kW	Δ*G*, kW	Δ*H*, kW
A	6	0.07206	−1135	−1095		
B	1	0.07206	−1778	−805.4	−642.6	289.7
C	9	0.07206	−1811	−799.5	−32.89	5.912
D	10	0.07206	−1091	193.3	720.3	992.9
E	2 + 3	0.07206	−1057	193.3	34.07	0
F	7 + 3	0.07206	−594.9	104.6	461.7	−88.7
G	8 + 3	0.07206	−545.5	104.6	49.33	0
H	8 + 4	0.07206	−200.8	55.57	344.8	−49.06
I	8 + 5	0.07206	−176.1	55.57	24.67	0

Note: columns: PTC—points of thermodynamic cycle, WM—working media.

3.6. Parameters of the points of thermodynamic cycle (hydrogen option)

Flow rates and composed thermodynamic potentials of the cycle points are shown in columns *m, G* and *H* of **Table 4**. Their pointwise increments are in columns Δ*G* and Δ*H*.

3.7. Characteristics of thermodynamic cycle (hydrogen option)

Table 4 shows that between points A and C, the heating of the system goes on. The transfer to point D is a properly electrochemical process of electrolysis, which needs the electric power $d_G = \Delta G_D$ and the addition of heat up to $d_H = \Delta H_D$. Assuming in the Equation (1) $k = 1.387$ (load factor, parameter of the imperfection of the electrochemical reaction), we get the power of the electrolyzer in accordance with Equation (2).

So, the total power of installation is composed of the following items (in kW):

- electrolyzer 998.8
- oxygen compressor 43.5
- hydrogen compressor 87.5
- electric boiler 45.4

Total 1175

4. Backup conversion methane-energy

4.1. Computational lay-out of the conversion of chemical energy of methane

An overview of the computational configuration adopted for the installation enabling backup methane-energy conversion is provided in **Figure 3**.

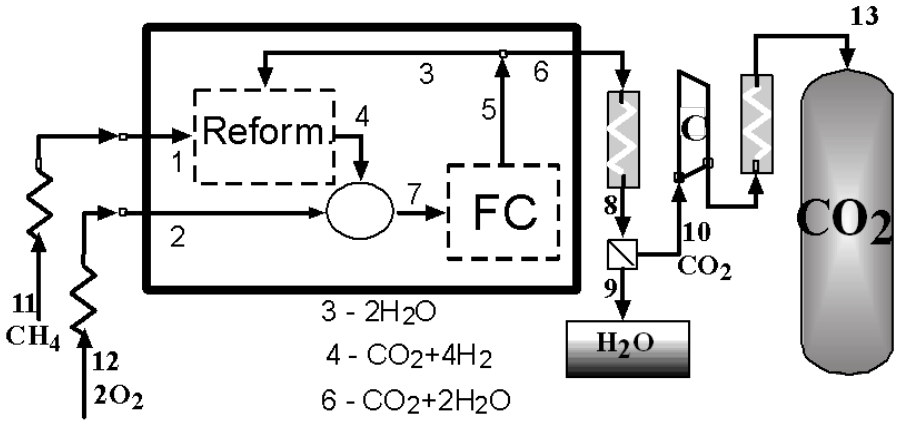

Figure 3. Computational lay-out of the installation for the backup conversion methane-energy.

4.2. Parameters of working media of the installation

Table A3 of **Appendix A** specifies the parameters of working media.

4.3. Parameters of TQ-diagrams of heat sources

Table 5 summarizes the parameters of the TQ diagrams characterizing the heat sources associated with the system illustrated in **Figure 3.**

Table 5. Characteristics of heat sources on **Figure 3**.

N	Working media	*m*, kg/s	*T1*, K	*T2*, K	*Q*, kW
1		1.0	1073	1073	96.44
2	6–8	0.08004	374.0	1073	87.57
3	10–13	0.04401	323.0	626.2	13.22
4	10–13	0.04401	323.0	554.3	9.839

Note:
Source 1 is what remains of the heat, created in the electrochemical reaction, after its internal use and the heating of inlet media at (11–1) and (12–2). Source 2 is the cooling of the mixture CO_2+steam at the indicated place of lay-out. Sources 3 and 4 appear due to the cooling after steps of compression.

4.4. Heat sinks

There are no heat sinks at the lay-out of **Figure 3**. All the heat from 4 sources will be delivered to the Stirling cycle for utilization.

4.5. Thermodynamic cycle of the process of conversion of chemical energy of methane into electricity

Identification of the points of thermodynamic cycle and of the involved working media is done in columns PTC and WM of **Table 6**.

Table 6. Thermodynamic cycle of backup conversion methane-energy.

PTC	WM	*m*, kg/s	*G*, kW	*H*, kW	Δ*G*, kW	Δ*H*, kW
A	12 + 11	0.08004	−209.7	−40.21		
B	2 + 11	0.08004	−568.2	10.91	−358.6	51.12
C	2 + 1	0.08004	−744.4	55.49	−176.2	44.58
D	2 + 4–3	0.08004	−812.8	246.7	−68.39	191.2
E	7–3	0.08004	−850.2	246.7	−37.36	0
F	5–3	0.08004	−1567	−746.1	−717.0	−992.9

Table 6. *Cont.*

PTC	WM	***m*, kg/s**	***G*, kW**	***H*, kW**	**Δ*G*, kW**	**Δ*H*, kW**
G	6	0.08004	−1562	−746.1	5.286	0
H	8	0.08004	−1070	−833.7	492.1	−87.57
I	9 + 10	0.08004	−1064	−833.7	5.938	0
J	9 + 13	0.08004	−1040	−835.7	23.53	−2.007

Note: columns: PTC—points of thermodynamic cycle, WM—working media.

4.6. Parameters of the points of thermodynamic cycle of conversion of chemical energy of methane

Flow rates and composed thermodynamic potentials of the cycle points are shown in columns *m, G* and *H* of **Table 6**. Their pointwise increments are in columns Δ*G* and Δ*H*.

4.7. Characteristics of thermodynamic cycle of conversion of chemical energy of methane

The following processes are going on between the points of thermodynamic cycle: AB—heating of oxygen, BC—heating of methane, CD—internal conversion of methane, DE—mixing of conversion products with oxygen, EF—electrochemical reaction, FG—recirculation of steam, GH—cooling of the mixture CO_2 + steam, HI—separation of steam, IJ—compression and cooling of CO_2.

The process EF (electrochemical oxidation of conversion products) ideally is capable of producing 992.9 kW of power, including electric power $N_{el} = -k\Delta G_F$. Assuming k = 0.85, one gets N_{el} = 609.5 kW. The heat output becomes $Q_{el} = \Delta H_F - N_{el}$. From this amount, a part, equal to ΔH_D=191.2 kW, is being consumed by the internal conversion of methane. The remains, together with heat sources 2 and 3, amount to 207.1 kW. When utilized in the Stirling cycle with efficiency according to Equation (3), they give 71.54 kW of additional power.

So, the total power of installation is composed of the following items (in kW):

– fuel cell 609.5
– CO_2 compressor −21
– heat utilization 71.54

Total 660

This power output, related to the power consumption during the direct conversion to methane (994.9 kW), gives the efficiency of the reciprocal process—0.6634.

5. Backup conversion hydrogen-energy

5.1. Computational lay-out of the fuel cell on hydrogen

The installation for backup conversion of the chemical energy of hydrogen into electricity is represented through its computational lay-out in **Figure 4.**

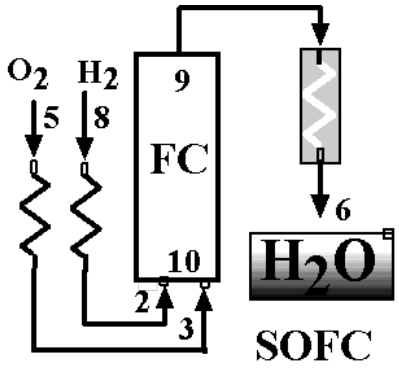

Figure 4. Computational lay-out of the installation for the backup conversion hydrogen-energy.

5.2. Parameters of working media of the fuel cell on hydrogen

Table A4 of **Appendix A** specifies the Parameters of working media.

5.3. Parameters of TQ-diagrams of heat sources of the fuel cell on hydrogen

For the system depicted in **Figure 4**, the characteristics and TQ-diagram parameters of the heat sources are provided in **Table 7**.

Table 7. Characteristics of heat sources on **Figure 4**.

N	Working media	*m*, kg/s	*T1*, K	*T2*, K	*Q*, kW
1		1.0	1073	1073	236.7
2	9–6	0.07206	374.0	1073	106.2

Note:
Source 1 is what remains of the heat, created in the electrochemical reaction, after its internal use. Source 2 is the cooling of the steam at the indicated place of lay-out.

5.4. Heat sinks of the fuel cell on hydrogen

There are no heat sinks at the lay-out of **Figure 4**. All the heat from 2 sources will be delivered to the Stirling cycle for utilization.

5.5. Thermodynamic cycle of the fuel cell on hydrogen

Identification of the points of thermodynamic cycle and of the involved working media is done in columns PTC and WM of **Table 8**.

Table 8. Thermodynamic cycle of backup conversion hydrogen-energy.

PTC	WM	*m*, kg/s	*G*, kW	*H*, kW	Δ*G*, kW	Δ*H*, kW
A	8 + 5	0.07206	−219.0	49.46		
B	2 + 5	0.07206	−698.0	142.2	−479.0	92.75
C	2 + 3	0.07206	−1057	193.3	−358.6	51.12
D	10	0.07206	−1091	193.3	−34.07	0
E	9	0.07206	−1811	−799.5	−720.3	−992.9
F	6	0.07206	−1200	−905.7	611.4	−106.2

Note: columns: PTC—points of thermodynamic cycle, WM—working media.

5.6. Parameters of the points of thermodynamic cycle of the fuel cell on hydrogen

Flow rates and composed thermodynamic potentials of the cycle points are shown in columns *m, G* and *H* of **Table 8**. Their pointwise increments are in columns Δ*G* and Δ*H*.

5.7. Characteristics of thermodynamic cycle of the fuel cell on hydrogen

Here, the processes AB and BC are the heating of hydrogen and oxygen. CD is the isoenthalpic process of their mixing before the electrochemical reaction. Process DE is the isobaric-isothermal electrochemical process, generating electricity. The last step of EF is the process of cooling steam, the source 2 of heat for utilization.

Electric power of the fuel cell according to the formula $N_{el} = -k\Delta G_E$ under $k = 0.85$ is equal to 612.3 kW.

From the thermal power $Q_{el} = \Delta H_E - N_{el}$, after its expenditure for the heating of hydrogen and oxygen, there remain 342.9 kW for utilization. Doing it in the Stirling cycle with efficiency according to Equation (3), one gets 136.3 kW of additional power. The total power amounts to 764.1 kW. This power output, related to the power consumption during the electrolysis (1175 kW), gives the efficiency of the reciprocal process—0.65.

6. Comparison of energy storage systems using methane and hydrogen as storage gas

Thermodynamic analysis of schemes at **Figures 1–4** allows a comparison of systems of indirect energy storage, realizing Power-to-Gas technology, that is producing the fuel during times of ample power supply and converts it back to electricity during periods of limited power supply, in two cases, when storage gases are methane and hydrogen. In both cases, the initial process of energy-gas conversion is the high-temperature electrolysis. In the case of methane electrolysis, hydrogen is used in the methanation process of CO_2, saved during the backup conversion of methane to energy. Backup gas-energy conversion in both cases is done in a solid oxide fuel cell.

Characteristics of these two energy storage systems are displayed in **Table 9** for the equal flow rates of hydrogen in reciprocal processes. The same is true for oxygen. In the methane case, there are two gases to save—methane and carbon dioxide. The total consumption of compressors for pumping them into 100 atm vessels is only half of the value, corresponding to hydrogen.

Table 9. Characteristics of energy storage systems for two storage gases.

Storage gas	**Methane**	**Hydrogen**
Energy consumption during the accumulation time (kW)		
Electrolyzer	998.8	998.8
Oxygen compressor	43.5	43.5
Methane compressor	20.08	
Hydrogen compressor		87.5
Heat utilization	−67.46	

Table 9. *Cont.*

Storage gas	Methane	Hydrogen
Electric boiler		45.4
Total	994.9	1175
Energy delivery (kW)		
SOFC	609.5	612.3
CO_2 compressor	−21	
Heat utilization	71.54	136.3
Total	660	764.1
Storage efficiency	0.6634	0.65

There are differences in the heat balance. In the regime of charge (times of ample power supply), in the methane case, there is an additional power of 67.46 kW from the heat utilization. In the hydrogen case, the direct conversion of 45.4 kW of electricity into heat is necessary. In the regime of discharge hydrogen case gives greater power from heat utilization. It means only that more heat is dumped.

In the scope of the current analysis, the adequate thermodynamic parameter to compare the presented options in **Table 9** is the storage efficiency, determined as the ratio of discharged and stored electricity.

7. Conclusion

A novel thermodynamic toolset is used to compare two systems of indirect energy storage in the scope of Power-to-Gas technology, with methane and hydrogen as storage gases. The comparison results in the conclusion that, in spite of the complexity, the methane option has some advantages.

1. The storage efficiency, determined as the ratio of discharged and stored electricity, is 0.6634 against 0.65 in the hydrogen option. Two cases of internal use of the developed heat might serve as an explanation of this fact:
   - During the energy storage, the heat of methanation is used to prepare the steam for electrolysis;
   - During the delivery of energy by SOFC, the internal conversion of methane is going on at the expense of the heat generated by the electrochemical reaction.
2. In spite of the additional necessity to store the carbon dioxide in the methane option, the joint methane and carbon dioxide compressor power is two times less compared with the corresponding value for hydrogen. There is a great experience to keep methane (rather than natural gas) in vessels. Hydrogen storage is hazardous. Until now isn't forgotten the accident with the dirigible "Hindenburg".

Even considering that the figures in this work are results of very strong assumptions, first of all, of the one-way conversion approach, they stimulate further investigations in the field of electricity storage into methane. In any case, the experience of dealing with the reaction of methanation, attained on earth, might be useful in the

cosmos. Just now, NASA investigates the capabilities of the Sabatier reaction to restore water from the carbon dioxide of expired air. It is important for ISS and future missions. Accompanying product of reaction (methane) will probably be dumped into cosmic space, and together will be dumped one half of hydrogen, which is the inlet reagent. There would arise the necessity of delivering hydrogen from Earth. All the same, there would be closed cycle of water, oxygen, and carbon dioxide.

Author contributions: Conceptualization, PI and AZ; methodology, PI; software, PI; writing—original draft preparation, PI; writing—review and editing, AZ; supervision, AZ. All authors have read and agreed to the published version of the manuscript.

Funding: No external funding.

Institutional review board statement: Not applicable.

Informed consent statement: Not applicable.

Data availability statement: The data used in this study are available from the corresponding author upon reasonable request.

Conflict of interest: The authors declare no conflict of interest.

References

1. Görtz J, Aouad M, Wieprecht S, et al. Assessment of pumped hydropower energy storage potential along rivers and shorelines. Renewable and Sustainable Energy Reviews. 2022; 165: 112027.
2. Rabi AM, Radulovic J, James M et al. Comprehensive review of compressed air energy storage (CAES) technologies. Thermo. 2023; 3(1): 104–126. doi: 10.3390/thermo3010008
3. Olabi A, Wilberforce T, Ramadan M, et al. Compressed air energy storage systems: Components and operating parameters—A review. Journal Energy Storage. 2020; 34: 102000.
4. Bazdar E, Sameti M, Nasiri F, et al. Compressed air energy storage in integrated energy systems: A review. Renew. Renewable and Sustainable Energy Reviews. 2022; 167: 112701.
5. Buttler A, Spliethoff H. Current status of water electrolysis for energy storage, grid balancing and sector coupling via power-to-gas and power-to-liquids: A review. Renewable and Sustainable Energy Reviews. 2018; 82(3): 2440–2454. doi: 10.1016/j.rser.2017.09.003
6. Ghorbani B, Salehi G, Ebrahimi A, et al. Energy, exergy and pinch analyses of a novel energy storage structure using post-combustion CO_2 separation unit, dual pressure Linde-Hampson liquefaction system, two-stage organic rankine cycle and geothermal energy. Energy. 2021; 233: 121051.
7. Ebrahimi A, Ghorbani B, Taghavi M. Novel integrated structure consisting of CO_2 capture cycle, heat pump unit, Kalina power, and ejector refrigeration systems for liquid CO_2 storage using renewable energies. Energy Science & Engineering. 2022; 10(8):3167–3188.
8. Taghavi M, Salarian H, Ghorbani B. Economic evaluation of a hybrid hydrogen liquefaction system utilizing liquid air cold recovery and renewable energies. Renewable Energy Research and Applications. 2023; 4(1):125–143.
9. Taghavi M, Salarian H, Ghorbani B. Thermodynamic and exergy evaluation of a novel integrated hydrogen liquefaction structure using liquid air cold energy recovery, solid oxide fuel cell and fotovoltaic panels. Journal of Cleaner Production. 2021; 320: 128821 doi: 10.1016/j.jclepro.2021.128821
10. Lehner M, Tichler R, Steinmüller H, et al. The power-to-gas concept. In: Lehner M, Tichler R, Steinmüller H, et al. (editors). Power-to-Gas: Technology and Business Models. Springer Briefs in Energy; 2014. pp. 7–17. doi: 10.1007/978-3-319-03995-4_2
11. Mueller M, Klinsmann M, Sauter U, et al. High temperature solid oxide electrolysis—technology and modeling. Chemie Ingenieur Technik. 2024; 96 (1–2): 143–166; doi: 10.1002/cite.202300137
12. Wendel CH, Gao Z, Barnett SA, et al. Modeling and experimental performance of an intermediate temperature

reversible solid oxide cell for high-efficiency, distributed-scale electrical energy storage. Journal of Power Sources. 2015; 283: 329–342. doi: 10.1016/j.jpowsour.2015.02.113
13. Wang W, Wang S, Ma X, et al. Recent advances in catalytic hydrogenation of carbon dioxide. Chemical Society Reviews. 2011; 40: 3703–3727.
14. Gao J, Wang Y, Ping Y, et al. A thermodynamic analysis of methanation reactions of carbon oxides for the production of synthetic natural gas. RSC Advances. 2012; 2: 2358–2368.
15. C. Molinet-Chinaglia C, Shafiq S, Serp P. Low Temperature Sabatier CO_2 Methanation. CheCatChem. 2024; 16(24). doi: 10.1002/cctc.202401213
16. Lin Y, Zhang W, Machida H, et al. CFD simulation of the Sabatier process in a shell-and-tube reactor under local thermal non-equilibrium conditions: Parameter sensitivity and reaction mechanism analysis. International Journal of Hydrogen Energy. 2022; 47(34): 15254–15269
17. HELMETH. HELMETH Project. Available online: http://www.helmeth.eu/ (accessed on 31 March 2025).
18. HELMETH. Methanation process. Available online: http://www.helmeth.eu/index.php/technologies/methanation-process (accessed on 31 March 2025).
19. HELMETH. Final Report Summary—HELMETH (Integrated High-Temperature Electrolysis and Methanation for Effective Power to Gas Conversion). Available online: https://cordis.europa.eu/project/id/621210/reporting (accessed on 31 March 2025).
20. HELMETH. Attachments (publishable figures) to final publishable report. Available online: https://cordis.europa.eu/docs/results/621/621210/final1-2017-03-01-helmeth-publishable-figures.pdf (accessed on 31 March 2025).
21. Leucht KW. How NASA will use robots to create rocket fuel on mars: the year is 2038. IEEE Spectrum. 2018; 55(11): 34–39. doi: 10.1109/MSPEC.2018.8513782
22. Zhuk AZ, Ivanov PP. Thermodynamic cycle of a solid oxide fuel cell with internal methane conversion under the one-way conversion approach. High Temperature. 2024; 62: 801–807. doi: 10.1134/S0018151X25700464
23. Zhuk AZ, Ivanov PP. Characteristics of a Solid Oxide Fuel Cell for the Thermodynamic Modeling of Power Plants. High Temperature. 2023; 61: 714–719.
24. Belov GV, Iorish VS, Yungman VS. Simulation of equilibrium states of thermodynamic systems using IVTANTHERMO for windows. High Temperature. 2000; 38(2): 191–196.
25. Curzon FL, Ahlborn B. Efficiency of a carnot engine at maximum power output. American Journal of Physics. 1975; 43: 22–24. doi: 10.1119/1.10023

Appendix A

Table A1. Parameters of working media at the **Figure 1**.

Working media	*p*, MPa	*T*, K	*m*, kg/s	*G*, kW	*H*, kW
1	0.1013	1038	0.07206	−1778	−11,177
2	0.1013	1073	0.008063	−596.7	15,558
3	0.1013	1073	0.064	−459.9	1061
4	0.1013	323.0	0.064	−115.2	294.1
5	10.0	323.0	0.064	−90.49	294.1
6	0.1013	288.0	0.07206	−1135	−15,197
7	0.1013	323.0	0.01604	−116.8	−3473
8	10.0	323.0	0.01604	−104.5	−3473
9	0.1013	1073	0.07206	−1811	−11,095
10	0.1013	1073	0.07206	−1091	2683
11	0.1013	323.0	0.03603	−580.0	−12,665
12	0.1013	323.0	0.05207	−702.0	−9833
13	0.1013	1073	0.05207	−1207	−7915
14	0.1013	1073	0.05207	−1258	−4243
15	0.1013	1073	0.04401	−639.4	−7870
16	10.0	323.0	0.04401	−440.5	−8699

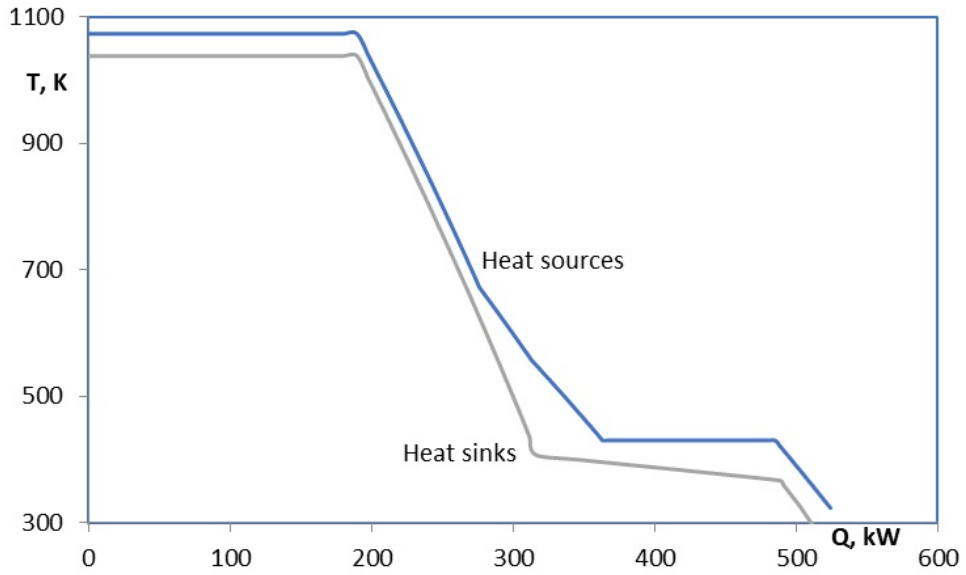

Figure A1. Composed TQ-diagrams for heat sources and heat sinks at **Figure 1**.

Table A2. Parameters of working media at the **Figure 2**.

Working media	*p*, MPa	*T*, K	*m*, kg/s	*G*, kW	*H*, kW
1	0.1013	1038	0.07206	−1778	−11,177
2	0.1013	1073	0.008063	−596.7	15,558
3	0.1013	1073	0.064	−459.9	1061
4	0.1013	323.0	0.064	−115.2	294.1
5	10.0	323.0	0.064	−90.49	294.1
6	0.1013	288.0	0.07206	−1135	−15,197
7	0.1013	323.0	0.008063	−134.9	4557
8	10.0	323.0	0.008063	−85.62	4557
9	0.1013	1073	0.07206	−1811	−11,095
10	0.1013	1073	0.07206	−1091	2683

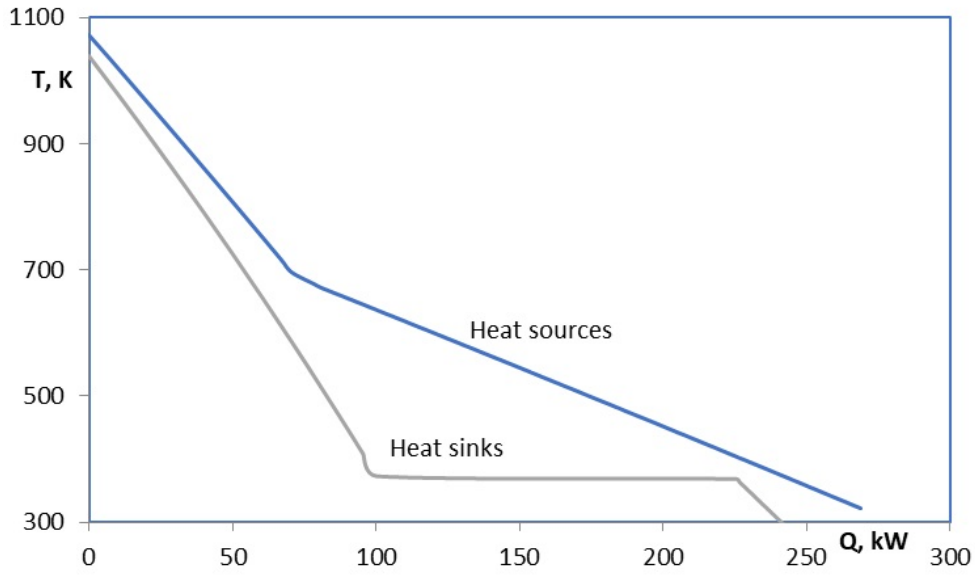

Figure A2. Composed TQ-diagrams for heat sources and heat sinks at **Figure 2**.

Table A3. Parameters of working media at the **Figure 3**.

Working media	*p*, MPa	*T*, K	*m*, kg/s	*G*, kW	*H*, kW
1	0.1013	1073	0.01604	−284.5	−772.9
2	0.1013	1073	0.064	−459.9	1061
3	0.1013	1073	0.03603	−905.5	−11,095
4	0.1013	1073	0.05207	−1258	−4243
5	0.1013	1073	0.1161	−2473	−9872
6	0.1013	1073	0.08004	−1562	−9322
7	0.1013	1073	0.1161	−1756	−1319
8	0.1013	374.0	0.08004	−1070	−10,416
9	0.1013	374.0	0.03603	−599.8	−12,569
10	0.1013	374.0	0.04401	−464.1	−8653
11	0.1013	288.0	0.01604	−108.3	−3551
12	0.1013	288.0	0.064	−101.3	262.0
13	10.0	323.0	0.04401	−440.5	−8699

Table A4. Parameters of working media at the **Figure 4**.

Working media	*p*, MPa	*T*, K	*m*, kg/s	*G*, kW	*H*, kW
2	0.1013	1073	0.008063	0	15,558
3	0.1013	1073	0.064	−459.9	1061
5	0.1013	288.0	0.064	−101.3	262.0
6	0.1013	374.0	0.07206	0	−12,569
8	0.1013	288.0	0.008063	−117.7	4055
9	0.1013	1073	0.07206	0	−11,095
10	0.1013	1073	0.07206	−1091	2683